

Design of a smart bidirectional actuator for space operation

Bortolino Saggin¹, Diego Scaccabarozzi^{1*}, Marco Tarbini¹, Marianna Magni¹, Carlo Biffi²,

Ausonio Tuissi²

¹ Politecnico di Milano, Polo Territoriale di Lecco, Via G. Previati 1c, 23900 Lecco (Italy)

² Istituto di Chimica della Materia Condensata e di Tecnologie per l'Energia, CNR, 23900 Lecco
(Italy)

* corresponding author: diego.scaccabarozzi@polimi.it

Abstract

A common need for space borne instruments, satellites and planetary exploration payloads is the usage of compact, light and low power actuators. In the recent years, this need has been partially solved by the development of customized solutions with an increasing usage of smart materials. A linear bidirectional actuator based on shape memory alloy technology is presented in this work. The device has been conceived to lock the double-pendulum scanning mechanism of a miniaturized Fourier transform spectrometer for planetary observation. The mechanism class is that of pin pullers, with the pin locking the movable components of the spectrometer during launch and landing phases. The proposed mechanism, differently from available off-the-shelf devices, allows multiple actuations without the need of manual resetting. Moreover, the device requires to be powered only to change its status. An appealing feature of the adopted concept is that the actuation is intrinsically shock-less, a key requirement for deployment of devices sensitive to mechanical vibration and shocks. All these characteristics, in addition to the design flexibility of the proposed concept in terms of achievable forces and strokes, make the designed actuator promising for many different applications, from space to ground. The designed bidirectional actuator provides 0.6 mm stroke and a 50 N preload but it represents just an example of implementation for the proposed concept. Structural design of the functional elastic components

25 and SMA alloy characterization have guided the actuator development. A mockup of the actuator
26 has been manufactured and the predicted performances preliminary validated.

27 **Keywords**

28 SMA, bidirectional actuator, compliant structure, resettable, pin-puller, holding mechanism, space
29 application, Mars, FTS.

30 **1 Introduction**

31 It is well recognized that SMAs provide some advantages in mechanisms and actuators design, i.e.
32 simplicity of related mechanisms, low driving voltage and sensing capability [1]. These
33 characteristics have been recently exploited in different fields, i.e. robotics [2], industry [3] and
34 aeronautics [4] to develop low power linear and rotational actuators. SMAs are very attractive for
35 space applications as well, where SMA technology usage is quite recent [5, 6] and mainly focused on
36 the actuation of deployable systems or damping system for spacecraft antennas [7]. In fact, SMAs
37 allow control of the deployment process and thanks to the shock-less actuation have been used for
38 developing low-shock release devices (LSRD). A clear advantage is that no additional damping is
39 required to suppress shocks and vibrations due to the deployment, unlike the systems based on elastic
40 energy storage. Example of space designed LSRD can be found in [8] where SMA and steel springs
41 work in contrast to achieve automatic resetting [9]. Some additional examples of LSRDs can be found
42 in [10-12], where SMA wires are used as triggers for the actuation. Moreover, thanks to the
43 advantages of the SMA technology, some recent customized spaceborne applications can be found in
44 gas release mechanism [13] or rock splitters [14].

45 The advantages of the SMA materials have been also exploited to develop low power linear and
46 rotational actuators [15]. Available spaceborne devices provide mass ranging between 4 and 40 g and
47 output force between 10 and 50 N. These actuators exploit SMA wire working against bias springs,
48 added to recover the initial configuration once SMA is not heated. This is a relevant limitation for a

49 general space application and in particular for instruments mounted on planetary rovers, given that
50 the deployed configuration requires a continuous power consumption.

51 Paraffin based actuator have been used in space as well, thanks to their reliability, large strokes (up
52 to 13 mm) and high forces (about 100 N). Unfortunately, the actuator mass is not negligible, no less
53 than 80g. Piezoelectric actuation has been evaluated as well among the existing solutions, thanks to
54 the accuracy of the output motion, the large stuck forces and the compatibility with low temperature
55 and vacuum environment. Anyway, the provided output displacement is generally limited to few
56 microns or, to achieve larger strokes, the actuator mass becomes quite large.

57 Thus, SMA technology was identified as the most promising for the development of an innovative
58 locking mechanism for the scanning pendulum of a miniaturized FT spectrometer 140x140x120 mm³
59 in size, 1 kg mass, designed to be mounted on a rover for Mars [16] . Holding was needed to keep the
60 pendulum in a safe position during launch and rover landing phases. This mechanism has become a
61 key component in any proposal for miniaturized FTS that has been conceived since then [17, 18]. As
62 evidenced by market and literature review, no multiple actuation devices compatible with our design
63 constraints are available, because they are either too massive or exceeding the size and power budgets.
64 Moreover, most of them are qualified down to -40°C, an operational limit not compatible with
65 environmental requirements for planetary surface operation. Exomars mission mechanical
66 environment had also challenging requirements due to the expected acceleration peak at landing on
67 Mars.

68 The developed actuator has many positive features: it provides two stable positions, requires power
69 only to change its status, uses only solid lubricants, can withstand at least one thousand working
70 cycles without relevant performances degradation and is capable of working at low temperatures. The
71 actuator concept is provided in the following whereas thermo-mechanical design is presented in
72 Section 2. SMA wire characterization and actuator preliminary testing are provided in Section 3 and
73 Section 4 eventually completes the paper.

74 *1.1 Actuator concept*

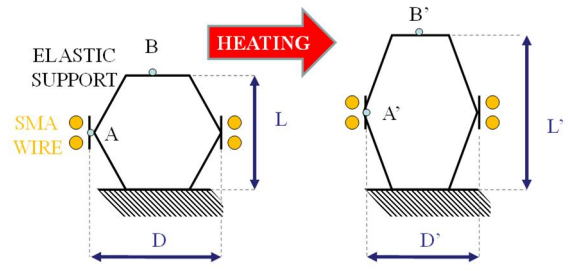
75 In order to understand the working principle of the proposed actuator two key points have to be
76 highlighted:

- 77 • Actuating force and displacement are provided by SMA wire contraction as consequence
78 of the material heating; and
- 79 • The actuator stroke is achieved by means of a displacement amplifier based on selectively
80 compliant element that amplifies the SMA wire contraction without frictional elements.

81 A sketch of the actuation concept is shown in Figure 1. SMA wire is wrapped around an elastic
82 support of diameter D and since the wire has been previously deformed, thanks to the material
83 memory effect [19], it recovers its original shape once heated. The wire contraction reduces the
84 support diameter and a new configuration (with diameter D') is achieved, resulting in the output
85 stroke provided by the actuator (as consequence, the elastic support extends from L to L'). The
86 concept is simple and reversible, since a pushing force applied to the elastic support stretches the wire
87 to its original configuration once the yield stress is exceeded.

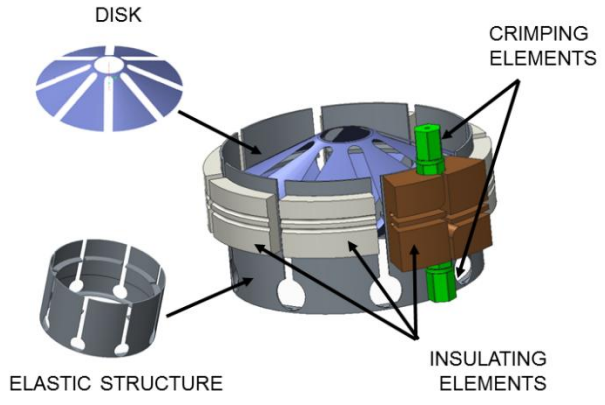
88 The elastic support design has a key role in the actuator performance since the output displacement
89 and force can be amplified by proper geometry selection. In SMA actuators design, displacement
90 amplification is a recurrent problem, developed mechanisms can be found in various references [20,
91 21]. Authors in [21] design a passive elastic system to increase the output stroke by about a factor 2.5
92 and achieve constant force during actuation. Mechanism proposed in literature cannot be
93 implemented in our case, because of our strict requirements of lightness, compactness and avoidance
94 of lubricants. Thus, the wire contraction amplification has been achieved with selectively compliant
95 element described in the next section. A preview of the final geometry is shown in Figure 2. The
96 elastic supports are derived from a thin disk slotted in eight sectors. Two disks are kept together by
97 an additional elastic structure that allows the initial positioning and avoid unwanted motions of the
98 disk sectors during the actuation. The proposed system has an intrinsic higher stability than planar

99 devices and allows the implementation of friction less joints, a mandatory requirement for space and
 100 vacuum applications. Thermally and electrically insulating sectors are glued over the cylindrical
 101 structure between the wire and the disks. These are cylindrical as well and guide the wires avoiding
 102 any axial sliding during the actuation. Finally, two crimping elements are used to transmit the wire
 103 load during the actuation.



104

105 **Figure 1 Actuation concept: wire heating varies elastic support geometry providing required output**
 106 **force and stroke.**



107

108
 109

Figure 2 Single-shot actuator 3D model.

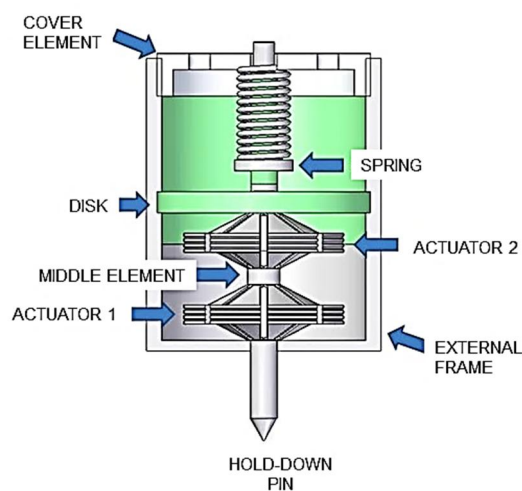
110 The system described in Figure 2 could be used alone as single shot actuator since it provides a stable
 111 open position once the SMA has been heated. However, no autonomous multiple actuations would
 112 be possible with this configuration because restoring of the initial position requires an external work.
 113 In resettable systems, this is achieved manually or in multiple actuations devices thanks to a bias
 114 spring that sets back the system when the SMA element cool down [15]. The latter configuration is
 115 simple and reliable but as previously mentioned, the need of power to keep the actuator in open
 116 configuration is often not acceptable, surely it would not be in our case where actuation would require

117 almost the whole instrument allocated power. Thus, in our design two single shot actuators are
118 mounted in opposition. By facing two components of the type of that in Figure 1, and playing with
119 the alternate powering of the two actuators, the final configuration allows either amplification of the
120 output stroke and realization of the bidirectional actuator.

121 1.2 Bidirectional actuator

122 A section view of the designed bidirectional actuator is shown in Figure 3. Different elements are
123 present:

- 124 • a hold-down pin locking the spectrometer pendulum; and
- 125 • a bias spring, providing the required preload on the pendulum; it has to be noticed that the
126 spring force is used only to provide the locking action and once the system is in open
127 position, it gives a static load to be overcome by the actuator 1; and
- 128 • two single-shot actuators facing each other; and
- 129 • SMA wire wrapped around the insulating supports; number of wires turns was determined
130 to be 2 for the bottom and 1 for the top actuators, respectively; and
- 131 • an aluminum frame, to complete the assembly.



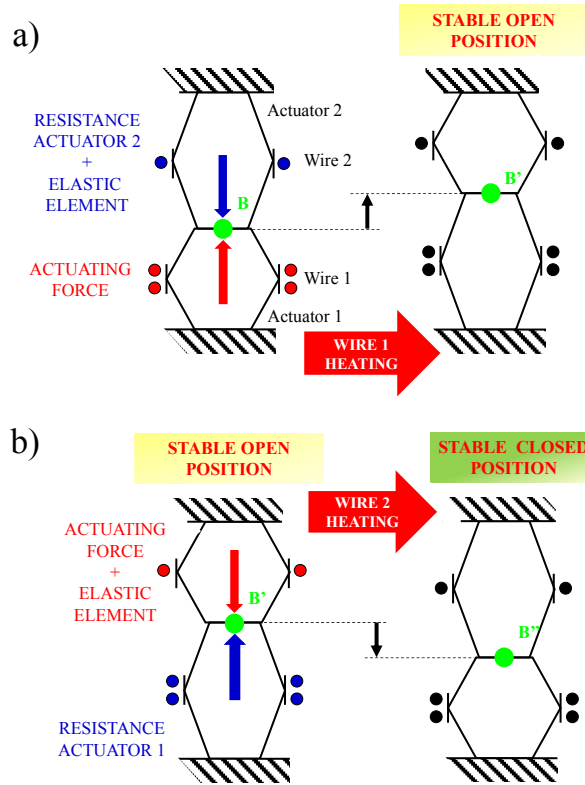
132

133

Figure 3 Section view of the bidirectional SMA actuator.

134

135 The two single-shot actuators (hereafter named actuator 1 and 2) are mounted in opposition to realize
136 the bidirectional configuration. Schematic of the intended opening/closing phases is shown in Figure
137 4.



138

139 **Figure 4 (a) Schematic of the actuation to achieve open stable position (b) backward actuation.**

140

141 When actuator 1 is heated, the hold-down pin moves upwards. A complete release is possible only if
142 actuator 1 overcomes the spring bias force and stretches actuator 2 wire. Once heating of the actuator
143 1 is switched off, the pin remains in the stable open position since the force provided by the bias
144 spring is lower than the one required to deform the wire 1. This is achieved by sizing the cross section
145 and number of wire turns of actuator 1.

146 Figure 4b shows the locking procedure. The system starts in the stable open position as result of the
147 previous actuation. Wire 2 is heated, recovering its shape and providing the force required to move
148 back the system. Wire 2 heating is switched off when actuator 1 is completely stretched back and the

149 hold-pin is locking the scanning mechanism. The bidirectional actuator is reset and ready for a new
150 cycle. In the following section detailed design of the single-shot actuator is provided. In particular,
151 disks geometry will be defined accounting for the motion phases and design requirements and the
152 single-shot actuator design will be optimized. To achieve required movement, actuator 1 and 2
153 comprise 2 and 1 turns of SMA wire, respectively.

154 **2 Thermo-mechanical design**

155 *2.1 Design requirements*

156 The actuator was originally developed for the Mars Infrared Mapper (MIMA)[22], a miniaturized
157 infrared spectrometer payload of the 2007 configuration of the ExoMars high-mobility rover
158 devoted to Mars surface observation. Unfortunately, a mission redesign aimed to mass and cost
159 reductions stopped MIMA development since the instrument mineralogical and atmospheric
160 science was regarded of minor importance with respect to the main exo-biologic mission's
161 objectives. Despite that, MIMA was a lucky pick-up for the mechanism requirements definition;
162 the extreme temperature range of the Martian environment, strict mass and power limitations of a
163 rover mounted instrument, the strong dynamic loadings due to the landing phase, the cleanliness
164 and shock-less request associated to the application on an interferometer, made it already
165 compatible with any following proposed usage [23]. Design requirements for the single-shot
166 actuator are summarized in the following:

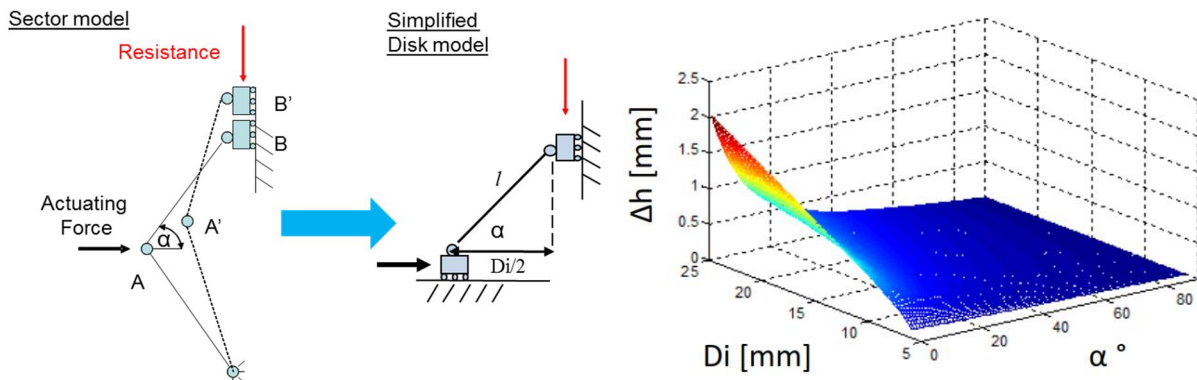
- 167 • A linear displacement of 0.6 mm to unlock the instrument scanning pendulum; and
- 168 • a holding force of 50 N, (required to warrant the locked position under the quasi-static
169 acceleration of 1000 m/s² at landing on Mars); and
- 170 • mass (derived from the single-shot off-the-shelf actuator) of 15 g and volume limited to
171 40x40x20 mm³; and
- 172 • 7W maximum power consumption; and

- 173 • survival temperature range between -120 and 40 °C, operating range between -80 and
- 174 40°C;
- 175 • no usage of organic lubricants.

176 2.2 Kinematic model

177 Forward kinematics allowed selection of the disk parameters to achieve required stroke, i.e. disk
 178 external diameter and initial inclination angle. Disks shown in Figure 2 are symmetrical, therefore
 179 two hinged rigid beams allow modelling the kinematic of each sector. The model is shown in
 180 Figure 4. Moreover, considering that a symmetry exists also in the horizontal plane of the actuator,
 181 the model is further simplified focusing on half actuator. Sketch of the simplified model is
 182 provided in Figure 5.

183



184

185 **Figure 5 (Left) single shot actuator kinematic model (right) computed vertical displacement vs disk**
 186 **size and initial inclination angle.**
 187

188 Knowing actuator geometry, i.e. inclination angle α and actuator diameter Di , vertical
 189 displacement is obtained as:

$$190 \Delta h = \sqrt{\left(\frac{Di}{2 \cos(\alpha)}\right)^2 - \left(\frac{Di}{2} - \Delta s\right)^2} - \frac{Di}{2} \tan(\alpha) \quad (1)$$

191 where Δs is the actuator radial displacement that depends on the SMA wire contraction. As worst
192 case, Δs was restrained to 2% of the initial radius. Moreover, this value allows up to 10^5 cycles of
193 actuation considering the SMA aging with cycling. Besides, this limit well above the required
194 value for the intended application and most locking devices. The static analyses performed are
195 bound to verify the feasibility of the proposed concept. In Figure 5, results of the kinematic
196 analyses shows that by increasing the wrapping diameter the output stroke increases as well.
197 Moreover, in order to maximize the amplification, disk inclination should be minimized. However,
198 minimizing the angle reduces the force exerted on the pin especially at the beginning of the
199 actuation. In fact, the force V (along the direction of the pin) and the radial one H (related to the
200 wire contraction), are linked by:

$$201 \quad H = \frac{V}{\tan(\alpha)} \quad (2)$$

202 where α is the inclination angle of the disk. Equation 2 has been used in the following to compute
203 tensile stress on SMA material in the different actuation phases. The trade-off between output
204 stroke and force led in our case to define the preliminary disk geometry with an inclination angle
205 of 27° and initial diameter of 25 mm. Un-deformed disk diameter was set 28 mm and the disk was
206 divided in 8 sectors. The kinematic analysis evidenced that even in the worst case of minimum
207 wire contraction (i.e. 2%), the actuator still provides the required output displacement of 0.6 mm.
208 This result had been verified in the following by FE analyses on the actuator. Models have been
209 developed with PTC Creo Simulate software © PTC Inc.

210 *2.3 Disk design*

211 Disks design has been performed developing a FE model based on shell elements (elements 4782
212 and 4610 nodes) as shown in Figure 6.

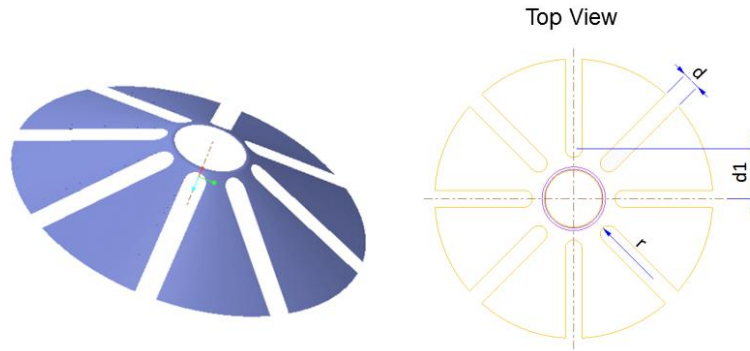


Figure 6 (Left) Disk FE model and (right) geometrical parameters.

Disk initial configuration has been selected by the simplified kinematic analyses presented above, in which the disk sectors were considered as stiff elements. Disk thickness and cuts have to be defined in order to completely define the disk geometry. Figure 6 shows remaining parameters to be defined. In order to warrant resistance against expected loads in operative condition, buckling analyses were performed. Maximum wire pull has been considered (i.e. 98 N), considering austenite plateau stress of manufacturer datasheet [24]. Half disk has been considered; displacements in the horizontal plane and rotations have been left free for the external diameters whereas hinge constraint has been applied at the inner disk circumference. Two different materials have been considered, aluminum (Al7075T6) and titanium (Ti6Al4V) alloys. Material characteristics are summarized in Table 1. Geometry of the disk has been varied in order to minimize disk stiffness. This has been achieved with optimization analyses having set maximum Von Mises stress for each material and minimum buckling coefficient, as for ECSS design [25].

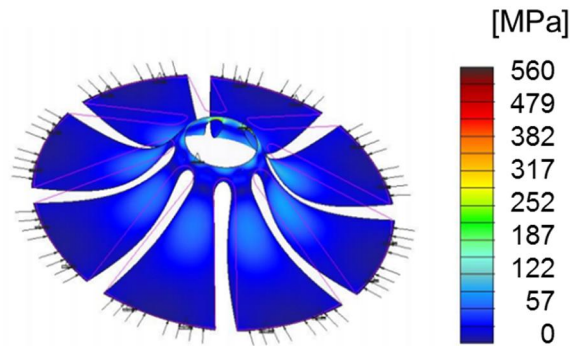
Material Property	Unit	Al 7075 T6	Ti6Al4V	Macor
Young Modulus	GPa	70	114	66.9
Density	kg/m ³	2800	4430	2520
Poisson Ratio		0.33	0.33	0.29
Ultimate Tensile Strength	MPa	572	950	345
Yield Tensile Strength	MPa	380	880	n.a.
thermal conductivity	W/(m K)	156	6.7	1.46

Table 1 Material properties of the FE model.

229 Optimization results are summarized in Table 2. Buckling Von Mises stress distribution is shown
 230 in Figure 7.

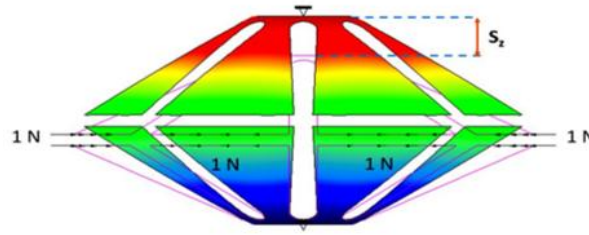
	Thickness [mm]	d [mm]	r [mm]	d1 [mm]
Optimization limits	0.35	1	0.5	3.5
	0.6	2	1	5
Ti6Al4V optimum	0.35	1.5	0.75	4
Al7075T6 optimum	0.38	1	0.5	4

231 **Table 2 Buckling analyses, geometry of the disks.**



232
 233 **Figure 7 Von Mises stress over the titanium disk, 0.35 mm thickness.**
 234

235 It can be seen that the titanium alloy allows for thinner elements. This is expected because of the
 236 higher mechanical strength and stiffness. In order to evaluate the force budget for the actuator
 237 feasibility verification, stiffness of the disk has been evaluated by means of FE model. In fact, the
 238 elastic deformation of the actuator due to the movement during wire contraction gives a resistance
 239 to be overcome. Two contributions are evaluated; these are related to the deformation of the disks
 240 once wire is recovering (upwards movement) or when a force from the top is applied (downwards
 241 movement). The latter force is present when actuator 2 is positioning back the pin. Thus, a FE
 242 model with two disks has been developed: disks have been matched with weighted links to allow
 243 relative rotation of the disks during the simulated conditions. A static analysis has been performed,
 244 with 1 N loading in radial direction. Deformed configurations is shown in Figure 8. In table 3 are
 245 summarized computed radial and vertical stiffnesses.



246
247 **Figure 8 Disks deformation with radial loading of 1N.**
248

Material	Radial stiffness [N/mm]	Axial stiffness [N/mm]
Ti6Al4V	5.15	10.26
Al7075T6	6.90	13.89

249 **Table 3 Single-shot actuator stiffnesses.**

250 Comparison between candidate materials allowed evidencing that titanium alloy is the chosen
251 material thanks to the lower axial stiffness while providing larger safety margin during actuation.

252 It has to be reminded that a complete actuation is defined by three different phases:

- 253 • Opening phase: the pin puller unlock the pendulum and open position is achieved; beside
254 the bias spring force, deformation of the disks and wire 2 deformation have to be overcome;
255 and
- 256 • Static phase: the system is stuck and the movement is prevented by the resistance to
257 deformation of wire 1; and
- 258 • Closing phase: the actuator 2 is activated, wire 1 is deformed again with the contribution
259 of the force due to the bias spring; the actuator is reset and ready for the next actuation
260 cycle.

261 According to ECSS design standard [25], friction force has to be considered with safety factor 3,
262 elastic ones have to be multiplied or divided by 1.2 depending on the role of resistance or motor in
263 the actuation. Forces can be computed for each phase and depend on the disk design, whose geometry

264 and material have been selected on the basis of the performed analyses. Resulting stresses in the final
265 configuration for the wires of the actuator 1 and 2 are summarized in Table 4. The detailed
266 computation of the stresses and the forces in each movement phase can be found in [26].

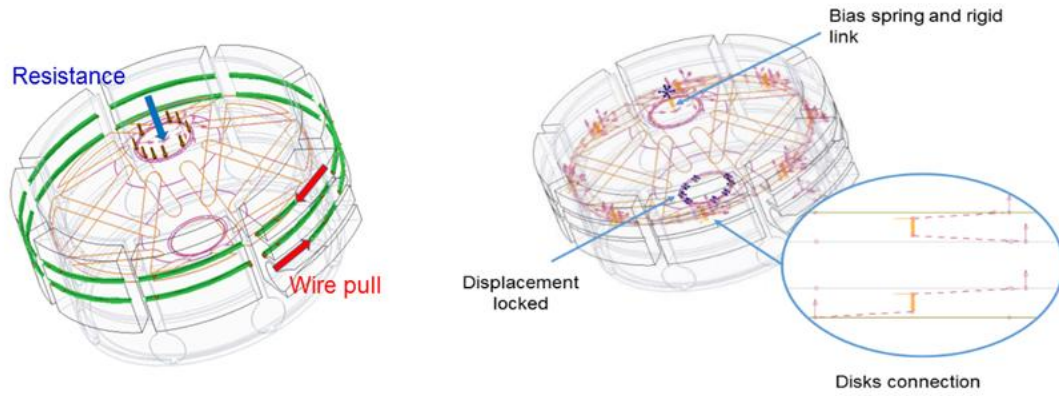
Movement Phase	Actuator 1	Actuator 2
	[MPa]	[MPa]
Opening	277.29	82
Static	59.92	0
Closing	82	335.98

267 **Table 4 Stress budget for actuator 1 and 2 wires.**

268 The analysis evidence that actuation is feasible for each phase, so the external reset is no longer
269 needed. In fact, austenitic and martensitic phases plateau stresses specified by SMA wire
270 manufacturer, ranging between 70 and 650 MPa, are compatible with required tensile stresses during
271 each actuation phase. Anyway, the SMA wire selected for the actuator development underwent an
272 individual characterization, which is described in the following.

273 *2.4 Actuator design*

274 A FE model of the actuator 1 was built in order to verify the output displacement based on solid
275 tetrahedrons and shell elements (44047 elements and 36708 nodes). The FE model comprises the two
276 identical disks linked together, the elastic structure and the insulating supports. As previously
277 mentioned, the rotation between the disks border is allowed. Forces and constraints are shown in
278 Figure 9. Resistance load of 133.5 N is applied on the actuator and a radial force of 70 N resulting
279 from the wire pull has been distributed over the insulating sectors.



280

281

282

Figure 9 Actuator FE model (left), lumped elements and constraints (right).

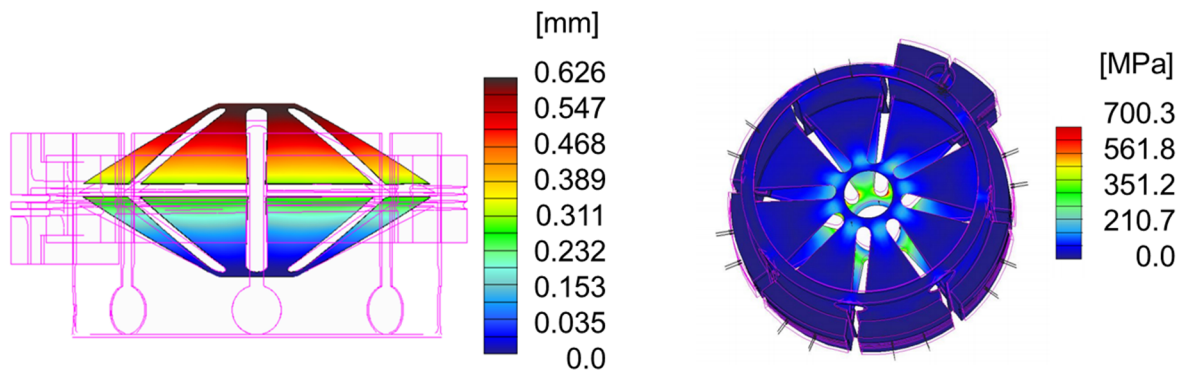
283

The bias spring has been added on the top of the actuator, as well. A single-shot actuator has been optimized using as cost function the maximization of the output displacement [27, 28]; disk parameters in Figure 5 are left free. Figure 10 provides output displacement with optimal configuration and Table 5 summarizes optimized disk geometry.

284

285

286



287

288

289

Figure 10 Actuator displacement (left) and Von Mises stress (right) during actuation phase.

Thickness [mm]	d [mm]	r [mm]	d1 [mm]
0.283	1	0.5	4.08

290

Table 5 Optimized single shot actuator parameters

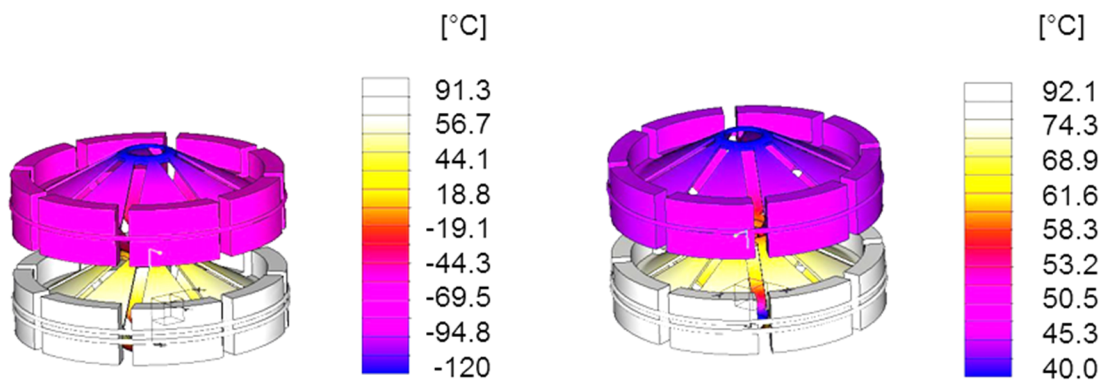
291

A thermal model of the actuator was developed with the aim of determining the power required to actuate the SMA wire in cryogenic condition. In fact, mission thermal analysis evidenced that in the case of cold Martian condition, expected lowest temperature is about -120 °C [23]. Actuators have

292

293

294 been thermally linked together by means of null thermal resistance in order to simulate the worst case.
 295 In fact, increasing the thermal resistance would reduce the power supply required for the actuation.
 296 Moreover, radiation heat exchange has been imposed on the disks, insulating supports and wire. The
 297 disks emissivity has been set to 0.05, assuming a gold coating of the titanium disks while unitary
 298 emissivity has been assumed for the insulating ceramic supports. In order to reduce the model
 299 complexity, wires have been modelled by separated circles on which heating has been uniformly
 300 distributed, simulating Joule heating effect. The two extreme conditions “cold” and “hot” have been
 301 analyzed; radiative and conductive interfaces have been set to -120°C and 40°C , respectively. The
 302 predicted temperature distributions in cold and hot cases are shown in Figure 11. The transformation
 303 temperature of 90°C is achieved on actuator1 heating the wire with 1.86 and 0.62 W, for cold and hot
 304 case respectively. These values are fully compliant with the mission requirements. Moreover, it can
 305 be seen that in the simulated cases temperature of the wire2 is always by far than the one required for
 306 complete austenite transformation, so there is no risk of simultaneous actuation of the two wires that
 307 would lead to a failure.
 308 Final configuration for the single shot actuator has 7g mass and radial size of 34 mm and height of
 309 15mm.



310

311

312

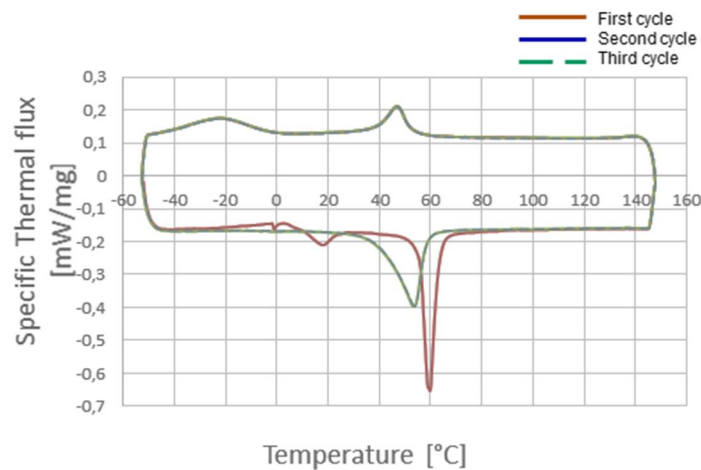
Figure 11 Temperature distribution with cold case (left) and hot case (right) testing.

313 **3 Experimental activity**

314 **3.1 Wire characterization**

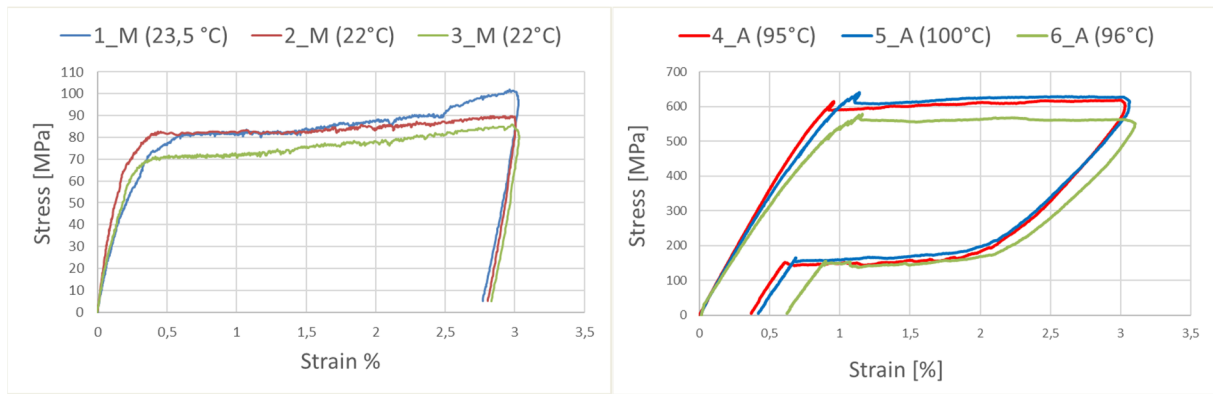
315 SMA wire from Memory-metalle GmbH/ Saes Group has been purchased for the actuator
316 development. Material characteristics have been measured to identify the transformation
317 temperatures in operative conditions and the stress-strain curves for the material different phases.

318 DSC Seiko calorimeter model 220 has been used for the calorimetric characterization. DSC samples
319 with 20 mg mass have been tested between -50 and 150°C. Temperature variation has been performed
320 with 10 °C/min rate and three cycles have been done. Specific heat flux curves are provided in Figure
321 12.



322
323 **Figure 12 Results of the DSC testing.**
324

325 MTS testing facility allowed functional testing to determine stress-strain curves in the martensitic and
326 austenitic phases. Material austenitic and martensitic states had been obtained by means of thermal
327 chamber at high (about 100 °C) and low (about RT) temperatures respectively. Tensile
328 loading/unloading cycles were performed, at constant temperatures, with 25 mm strain gauge
329 extensometer and a preload of 2N. Deformation rate was set to 2 mm/min with maximum deformation
330 of 3%. Temperature variation between 22 and 24 °C was accepted for the martensite testing whereas
331 95°C was the kept as minimum for the austenitic phase characterization. Results of the tensile tests
332 are shown in Figure 13.



333

334

335

Figure 13 Functional testing: martensitic (left) and austenitic (right) states.

336

Table 6 provide mechanical characteristics derived from stress-strain curves.

Test ID	Elastic Modulus [GPa]	Plateau Stress [MPa]
1_M	28	80
2_M	43	80
3_M	30	70
4_A	73	602
5_A	70	628
6_A	63	560

337

Table 6 DSC and functional testing transformation temperatures. Units are °C.

338

Strain recovery heating/cooling loops, under constant load (simulating working condition with dead

339

mass of 5 kg, i.e. nominal tensile stress of 250 MPa) and temperature cycling has been performed in

340

a thermal chamber (ACS Angenlanti Industrie type), equipped with a LVDT (Linear variable

341

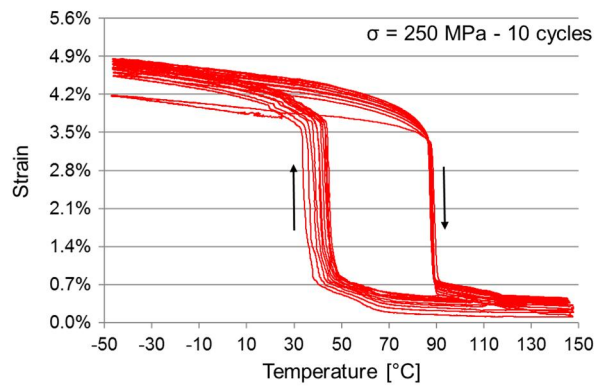
differential transducer) to measure the wire deformation under heating and cooling. Temperature

342

variation rate was set to 2°C/min between -50 and 150 °C and 10 cycles between minimum and

343

maximum temperatures had been performed. Results are shown in Figure 14.



344
345 **Figure 14 Functional testing: strain vs temperature.**
346

347 Obtained transformation temperatures are compared with DSC results in Table 7.

Temperatures	DSC	1 st cycle	2 nd cycle	10 th cycle
Ms	-3.6	38.46	38.51	46.52
Mf	-45	32.34	35.68	43.20
As	39	87.31	87.07	85.74
Af	57	89.63	88.61	87.66

348 **Table 7 DSC and functional testing transformation temperatures. Units are °C.**

349 3.2 Discussion

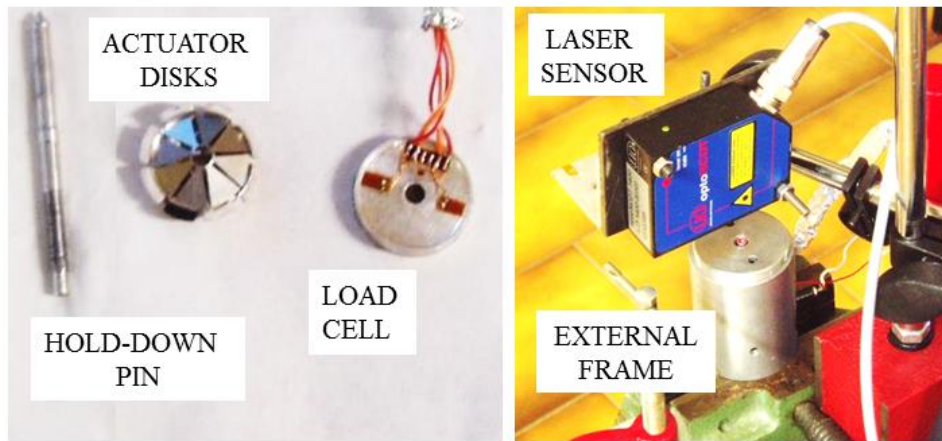
350 Heat peaks in Figure 12 identify phase transformation temperatures. During cooling two peaks have
351 been found, since between martensite and austenite the phase R is present. During heating just one
352 peak is found since the transformation peaks are coincident. Transformation temperatures,
353 summarized in Table 7, have been derived looking to the intersection between the tangent of the DSC
354 curves at the measured peaks. Austenitic phase is achieved at relatively low temperature, about 60
355 °C. This is important for our design, since a low heating power is expected even in cryogenic
356 condition (as confirmed by thermal modelling). As expected, for a non-trained wire, there is not a
357 thermal cycling stability particularly for the firsts heating/cooling cycles (see DSC cooling curves)
358 [29]. However, after three DSC scans a stabilization is achieved. Typical thermal hysteresis (about
359 40°C) of NiTi wire for shape memory application is shown also.

360 Figure 13 depicts mechanical behaviors of the material and the characteristic plateaus related to the
361 de-twinning of the martensite (low temperature) and stress induced martensite (high temperature) are
362 well shown. Mechanical modulus as well as stresses plateau values are summarized in Table 6. It can
363 be seen that measured values are compatible with datasheet specifications and are in agreement with
364 previous literature studies. For the martensitic phase the elastic modulus varies between 28 and 43
365 GPa and plateau stress is varying between 70 and 80 MPa. For the austenitic phase, the elastic
366 modulus and plateau stress increase up to 70 GPa and 600 MPa, respectively. Worst case combination
367 of the measured mechanical properties had been used in the feasibility and optimization design
368 phases.

369 Finally, except for the first cycle, the wire under constant load of 250 MPa exhibits a stable functional
370 performance after few heating/cooling cycles (see Figure 14). This means that with proper training
371 (lasting no more than 10 cycles), the wire is ready for the actuation. Another important behavior is
372 that the transformation temperatures change as consequence of the applied stress. Table 7 evidences
373 that a general increase of the temperature is obtained. In particular, M_f is about 40°C and A_f achieves
374 87 °C. The latter values had been used as reference for the design described in Section 2.

375 3.3 *Actuator Testing*

376 With the aim of verifying the design and highlighting drawbacks and possible improvements, a
377 mock-up for the single actuator has been realized. Figure 15 shows the single-shot actuator
378 breakdown and the experimental setup.



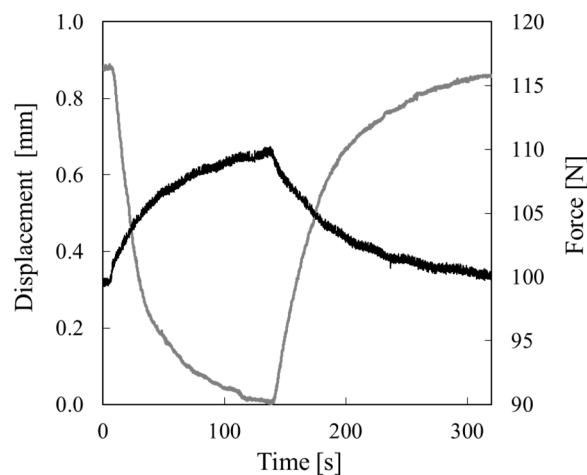
379

380
381

Figure 15 Actuator breakdown, load cell and experimental setup for the actuator testing.

382
383
384
385
386
387

Actuating force was measured by a load cell (range 150 N, linearity 0.5% of the measurement range) mounted between the hold-down pin and the ground. Displacement has been measured by laser Micro Optronic ILD 1400-05 (range 5mm, maximum linearity error 9 μm). The single-shot actuator was loaded with a dead mass of 10 kg (as worst case loading) and powered with a constant current of 1.8 A, value was selected to achieve complete transformation but avoid the wire overheating. Figure 16 shows measured force and displacement during an actuation cycle.



388

389
390

Figure 16 Measured displacement (grey color) and force (black) of the single actuator.

391
392
393

Once that the actuation starts, the hold-down pin reaches the maximum displacement of 0.9 mm after about 140 s. This is confirmed by the load increasing, due to the spring element, up to 110 N.

394 Once the electrical power is switched off, the system comes back to the initial position in about
395 three minutes. This is expected since the load is larger than the one that causes system closing.
396 Moreover, the measured stroke is higher than the nominal 0.6 mm. This result was expected too,
397 because the actual SMA recovery was larger than the 2% value, assumed as end of life figure in
398 the design. This happened despite the wire had been “aged” with more than 1000 cycles.

399 The obtained result evidenced the need of an accurate control of the actuator geometry and wire
400 contraction, to match the expected performances. As positive outcome, the obtained result also
401 highlighted the intrinsic flexibility of the proposed concept that can be adjusted to different
402 displacement requirements with small changes of the starting wire length.

403

404 **4 Conclusions**

405 A light and small bidirectional actuator was designed to lock the mechanism of a miniaturized infrared
406 spectrometer. The actuator is based on SMA technology and can provide 0.6 mm output displacement
407 against 50 N loading. The actuator is based on elastic structures whose geometry can be changed to
408 face different requirements in terms of force or displacement, which amplify the contraction of the
409 SMA wire. The bidirectional working is achieved without requiring power either than that necessary
410 for the position commutation. Moreover, the actuator concept flexibility can be exploited to match
411 different working condition, i.e. by changing the wire diameter to achieve higher forces or the actuator
412 geometry to allow larger displacements. A commercially available wire has been selected and tested
413 to develop a mockup of the proposed actuator. Testing of the manufactured mockup allowed
414 preliminary validation of the proposed concept. **Future activity is foreseen to fully characterize the
415 designed actuator in terms of force vs displacement performance in more general working conditions;
416 this would enable evaluating the actuator suitability for applications different from the designed
417 locking system.**

418

419 **References**

420

- 421 1. J. M. Jani, M. Leary, A. Subic, and M. A. Gibson, "A review of shape memory alloy research,
422 applications and opportunities," *Mater Des* **56**, 1078-1113 (2014).
- 423 2. J. Sheng and J. P. Desai, "Design, modeling and characterization of a novel meso-scale SMA-
424 actuated torsion actuator," *Smart Mater. Struct.* **24**, 105005 (2015).
- 425 3. D. Patil and G. Song, "Shape memory alloy actuated accumulator for ultra-deepwater oil and gas
426 exploration," *Smart Mater. Struct.* **25**, 045012 (2016).
- 427 4. S. Barbarino, E. S. Flores, R. Ajaj, I. Dayyani, and M. Friswell, "A review on shape memory
428 alloys with applications to morphing aircraft," *Smart Mater. Struct.* **23**, 063001 (2014).
- 429 5. A. Razov and A. Cherniavsky, "Applications of shape memory alloys in space engineering: past
430 and future," *EUROPEAN SPACE AGENCY-PUBLICATIONS-ESA SP* **438**, 141-146 (1999).
- 431 6. E. M. Flint, J. Melcher, and H. Hanselka, "The 'promise' of smart materials for small satellites,"
432 *Acta Astronaut.* **39**, 809-814 (1996).
- 433 7. H. Oh, S. Jeon, T. Kim, and Y. Kim, "Experimental feasibility study for micro-jitter attenuation
434 of stepper-actuated X-band antenna-pointing mechanism by using pseudoelastic SMA mesh
435 washer," *Smart Mater. Struct.* **24**, 045010 (2015).
- 436 8. A. Peffer, K. Denoyer, E. Fosness, and D. Sciulli, "Development and transition of low-shock
437 spacecraft release devices," in *Aerospace Conference Proceedings, 2000 IEEE*, Anonymous (IEEE,
438 2000), pp. 277-284.
- 439 9. T. Georges, V. Brailovski, and P. Terriault, "Characterization and design of antagonistic shape
440 memory alloy actuators," *Smart Mater. Struct.* **21**, 035010 (2012).
- 441 10. F. Peng, X. Jiang, Y. Hu, and A. Ng, "Actuation precision control of SMA actuators used for
442 shape control of inflatable SAR antenna," *Acta Astronaut.* **63**, 578-585 (2008).
- 443 11. M. Lee, J. Son, H. Hwang, Y. Kim, and B. Kim, "Shape Memory Alloy (SMA) Actuator Based
444 Separation Device," (2011).
- 445 12. Y. I. Yoo, J. W. Jeong, J. H. Lim, K. Kim, D. Hwang, and J. J. Lee, "Development of a non-
446 explosive release actuator using shape memory alloy wire," *Rev. Sci. Instrum.* **84**, 015005 (2013).
- 447 13. R. Edeson, M. Whalley, B. Kent, S. Canfer, and E. Sawyer, "SMA gas release mechanism for
448 the Rosetta Lander's Ptolemy instrument," *Acta Astronaut.* **58**, 576-582 (2006).
- 449 14. O. Benafan, R. Noebe, and T. Halsmer, "Static rock splitters based on high temperature shape
450 memory alloys for planetary explorations," *Acta Astronaut.* **118**, 137-157 (2016).
- 451 15. Q. Donnelan, "Design and testing of linear shape memory alloy actuator," Final Report,
452 National Science Foundation—Research Experience for Undergraduates (2005).

- 453 16. B. Saggin, E. Alberti, L. Comolli, M. Tarabini, G. Bellucci, and S. Fonti, "MIMA, a
454 miniaturized infrared spectrometer for Mars ground exploration: Part III. Thermomechanical
455 design," in *Remote Sensing*, Anonymous (International Society for Optics and Photonics, 2007), pp.
456 67441S-67441S-10.
- 457 17. I. Shatalina, B. Saggin, D. Scaccabarozzi, R. Panzeri, and G. Bellucci, "MicroMIMA FTS:
458 design of spectrometer for Mars atmosphere investigation," in *SPIE Remote Sensing*, Anonymous
459 (International Society for Optics and Photonics, 2013), pp. 88900T-88900T-12.
- 460 18. B. Saggin, D. Scaccabarozzi, I. Shatalina, R. Panzeri, M. Tarabini, M. Magni, and G. Bellucci,
461 "MicroMIMA, a miniaturized spectrometer for planetary observation," in *Metrology for Aerospace*
462 (*MetroAeroSpace*), 2015 *IEEE*, Anonymous (IEEE, 2015), pp. 502-506.
- 463 19. H. Funakubo, "Shape Memory Alloys,(1987)," Gordon and Breach Science Pub1-60 (2008).
- 464 20. H. Ishii and K. Ting, "SMA actuated compliant bistable mechanisms," *Mechatronics* **14**, 421-
465 437 (2004).
- 466 21. G. S. Mammano and E. Dragoni, "Increasing stroke and output force of linear shape memory
467 actuators by elastic compensation," *Mechatronics* **21**, 570-580 (2011).
- 468 22. B. Saggin and D. Scaccabarozzi, "Design and optimization of the calibration procedure for a
469 miniaturized Fourier transform spectrometer," *Appl. Spectrosc.* **65**, 627-633 (2011).
- 470 23. D. Scaccabarozzi, B. Saggin, and E. Alberti, "Design and testing of a roto-translational shutter
471 mechanism for planetary operation," *Acta Astronaut.* **93**, 207-216 (2014).
- 472 24. Memory Metalle GmbH, "Info Sheet No 4, Selected Properties of NiTi-based Alloys,
473 http://www.memory-metalle.de/html/03_knowhow/PDF/MM_04_properties_e.pdf," .
- 474 25. ESA, "ECSS E30 Part 2 A, Mechanical—Part 2: Structural," .
- 475 26. G. Balatti, "Sviluppo di un attuatore bidirezionale per applicazione spaziale, MSc degree,
476 Polytechnic University of Milan, <https://www.politesi.polimi.it/handle/10589/109009>," (2015).
- 477 27. M. G. Gritti, H. Giberti, and A. Collina, "Optimal synthesis of a cam mechanism for train
478 pantograph," in *Mechatronics (ICM), 2013 IEEE International Conference on*, Anonymous (IEEE,
479 2013), pp. 406-411.
- 480 28. H. Giberti, S. Cinquemani, and S. Ambrosetti, "5R 2dof parallel kinematic manipulator—A
481 multidisciplinary test case in mechatronics," *Mechatronics* **23**, 949-959 (2013).
- 482 29. A. Tuissi, P. Bassani, A. Mangioni, L. Toia, and F. Butera, "Fabrication process and
483 characterization of NiTi wires for actuators." in *SMST-2004: Proceedings of the International*
484 *Conference on Shape Memory and Superelastic Technologies*, Anonymous (, 2006), pp. 501-508.
- 485